Engineering of NEMO as calcium indicators with ultra-high dynamics and sensitivity

Jia Li[*1], Ziwei Shang[*2], Jia-Hui Chen[*3], Wenjia Gu[*1], Li Yao[*2], Xin Yang[4], Xiaowen Sun[2], Liuqing Wang[1], Tingting Hou[5], Shi-Qiang Wang[5], Dajun Xing[2], Donald L. Gill[6], Lijuan Hou[4], Yubin Zhou[#7], Ai-Hui Tang[#3,8], Xiaohui Zhang[#2], Youjun Wang[#1,9]

[1] Beijing Key Laboratory of Gene Resource and Molecular Development, College of Life Sciences, Beijing Normal University, Beijing, 100875, China.

[2] State Key Laboratory of Cognitive Neuroscience & Learning, IDG/McGovern Institute for Brain Research, Beijing Normal University, Beijing, 100875, China. Email: xhzhang@bnu.edu.cn

[3] CAS Key Laboratory of Brain Function and Disease and Hefei National Research Center for Physical Sciences at the Microscale, Division of Life Sciences and Medicine, University of Science and Technology of China, Hefei 230026, China. Email: tangah@ustc.edu.cn

[4] Exercise physiology and Neurobiology Lab, College of P.E. and Sports, Beijing Normal University, Beijing, 100875, China.

[5] State Key Laboratory of Membrane Biology, College of Life Sciences, Peking University, Beijing, 100871, China.

[6] Department of Cellular and Molecular Physiology, Pennsylvania State University College of Medicine, Hershey, Pennsylvania 17033

[7] Institute of Biosciences and Technology, Texas A&M University, Houston, TX, 77030, USA. Email: yubinzhou@tamu.edu

[8] Institute of Artificial Intelligence, Hefei Comprehensive National Science Center, Hefei 230026, China

[9] Key Laboratory of Cell Proliferation and Regulation Biology, Ministry of Education, College of Life Sciences, Beijing Normal University, Beijing, 100875, China. Email: wyoujun@bnu.edu.cn

[*] These authors contributed equally to this work

[#] Corresponding authors

Abstract

Genetically-encoded calcium indicators (GECI) are indispensable tools for real-time monitoring of intracellular calcium signals and cellular activities in living organisms. Current GECIs are fraught with having sub-optimal peak signal-to-baseline-ratio (SBR) with limited resolution for reporting dynamic calcium transients. We report herein the development of a suite of calcium sensors, designated NEMO, with fast kinetics and ultra-wide dynamic ranges. NEMO indicators report Ca^{2+} transients with peak SBRs ~20-fold larger than the top-of-the-range GCaMP series. NEMO further enable the quantification of absolution calcium concentration with ratiometric or photochromic imaging. Compared to GCaMPs, NEMO could detect single action potentials in neurons with peak SBR twice higher and median peak-SBR four times larger *in vivo*, thereby, outperforming most existing state-of-the-art GECIs. Given their unprecedented high sensitivity and fast resolution for decoding intracellular Ca^{2+} signals, NEMO sensors may find broad applications in monitoring neuronal activities and other Ca^{2+}-modulated physiological processes.

The calcium ion (Ca^{2+}) is a messenger essential for life and death, mediating responses ranging from neurotransmitter release, muscle contraction, to gene expression. The information is encoded in transient three-dimensional changes of Ca^{2+} concentration in space, time, and amplitude (*1*). Genetically-encoded Ca^{2+} indicators (GECI) are indispensable tools for real-time monitoring of Ca^{2+} signaling and cellular activities, such as neuronal activation (*2*). The signal-to-background ratio (SBR; $\Delta F/F_0$)(*3*), defined as the ratio of the absolute fluorescence (F) changes ($F-F_0$, or ΔF) over the basal fluorescence (F_0), is a key parameter used to gauge the performance of mono-colored GECIs. Tremendous efforts have been devoted to generate GECIs with faster kinetics (e.g., jGCaMP8 series (*4*)), but progress toward increased maximal fluorescence change has remained relatively lagging since the development of GECO and GCaMP6 series approximately ten years ago(*5, 6*).

With a Ca^{2+}-sensing module installed within one fluorescent protein (FP), single-FP-based indicators use Ca^{2+}-dependent fluorescence changes to report Ca^{2+} transients. Calmodulin (CaM) together with its target peptide (for example, RS20 or M13) is the most commonly used Ca^{2+} sensing module. Two strategies have been generally applied to link CaM-M13 with FP: (i) GCaMP-like design (*6*) to install CaM and M13 to the C- and N-termini of a FP, like circular permutated enhanced green FP (EGFP); and (ii) NCaMP7-like strategy(*7*) to insert CaM-M13 into the middle of a FP(*8*). Over the past 20 years, modifications within the linkers and interaction interfaces among CaM, M13 and FP were proven successful strategies to improve the sensitivity, speed and dynamics of GCaMP variants(*4, 6, 9*). However, further improvements on their dynamic range are restricted by the brightness of EGFP. While NCaMP7 was built upon the brightest monomeric green FP, mNeonGreen (mNG) (*10*), it has a small *in cellulo* dynamic range with slow kinetics(*7*). By combining the advantages of both GCaMP and NCaMP7 series, we set out to develop substantially improved GECIs with fast speed and ultra-high dynamic ranges building upon mNG.

Engineering of mNeonGreen-based calcium indicators (NEMO)

Single-FP-based indicators share some structural similarities at the sensing module insertion

sites(*8*), and most GECI constructs use CaM-M13 as the Ca^{2+} sensing module(*11*). We therefore reasoned that the design and optimization strategies of CaM-based indicators might be transferable in principle among GECIs. We thus created a pool of constructs mostly by applying known GECI design strategies to mNG, and screened their performance in mammalian HEK 293 cells (**Fig. 1A–C**, **Supplementary Tables 1-2**).

We first evaluated the basal fluorescence (F_0) and the ratio between maximal (F_{max}) and minimal (F_{min}) fluorescence, or the dynamic range (F_{max}/ F_{min}), of the constructs. To allow measurements of F_{min}, endoplasmic reticulum (ER) Ca^{2+} stores in mammalian cells were depleted by incubating the cells in a Ca^{2+}-free buffer containing 300 μM EGTA and 1 μM thapsigargin (TG) for 10 min. TG is an inhibitor of sarcoplasmic/endoplasmic reticulum Ca^{2+} ATPase and can induce passive store depletion of ER. Following this, a high amount of Ca^{2+} (100 mM) was added to the culture medium to induce F_{max} via store-operated Ca^{2+} entry (SOCE) (**Fig. 1B-C**). Time-lapsed imaging was used to monitor store depletion-induced changes in cytosolic Ca^{2+} by using NCaMP7 and GCaMP6m as the references (**Fig. 1B**). Top candidates (**Fig. 1C**) were identified based on the F_0 and the dynamic range (F_{max}/F_{min}) values (**Fig. 1D**). We found that the GCaMP-like design (*6*) did not work out with mNG (**Supplementary Table 1**), while NCaMP7-like (*7*) variants (**Fig. 1A**) showed improved dynamics and speed (**Supplementary Table 2**). Among all the variants, we identified five best-performing constructs and named them as members of the mNeonGreen-based Calcium indicator (NEMO) family, including the medium (NEMOm), high contrast (NEMOc), fast (NEMOf), bright (NEMOb) and sensitive (NEMOs) versions (**Fig. 1D**, **Supplementary Fig. 1 and 2A**). We then analyzed their physiochemical properties and explored possible applications in more details.

Ex vivo characterization of NEMO sensors

Overall, the *in cellulo* dynamic range of NEMO sensors was superior to that of top-of-the-range GECI proteins tested. Compared with NCaMP7, NEMOs and NEMOb bear an extra N-terminal linker (L1) and harbor a single amino acid substitution (M324I) in the linker (L4) between M13 and mNG (**Fig. 1A**). The dynamic range of NEMOs or NEMOb (102.3 ± 4.0 or 128.8 ± 3.1,

correspondingly) was found to be at least 4.5 times higher than that of GCaMP6m or NCaMP7 (22.9 ± 0.3 and 15.8 ± 0.5, respectively) (**Fig. 1D**). In addition to the M324I mutation, NEMOm and NEMOc have additional modifications to the linker region between CaM and M13 (**Fig. 1A**). As a result, the dynamic ranges of these two indicators were further increased to 240.7 ± 7.6 and 422.2 ± 15.3, respectively, which were 9.5 to 25.7-fold higher than that of GCaMP6m or NCaMP7 (**Fig. 1D**, **Supplementary Movie 1**). To the best of our knowledge, NEMO indicators represent the first class of GECI sensors with an *in cellulo* dynamic range of over 100-fold.

To characterize Ca^{2+}-dependent properties of NEMO indicators more quantitatively, we performed *in vitro* Ca^{2+} titration experiments using recombinant NEMO proteins purified from bacteria. We found that NEMOc, NEMOf, and NEMOs showed dynamic ranges of 182, 128, and 100-fold, respectively (**Fig. 1E**). Although brightest in basal fluorescence among all NEMO variants, NEMOb only showed 66-fold change in the dynamic range, prompting us to focus on the other four variants for further characterization. Even though the Ca^{2+} binding affinity of NEMOs or NEMOm (155.8 ± 3.8 nM and 248.4 ± 3.7, respectively) remained comparable with GCaMP6m (206.4 ± 5 nM), the *in vitro* dynamic range was 3.2 to 5.6-fold higher than that of GCaMP6m (**Fig. 1E**). Hence, the high *in cellulo* dynamic range of NEMO sensors does not seem to be related to their Ca^{2+} affinities.

We next examined the basal fluorescence of NEMO sensors in HEK293 cells. We used a P2A-based bicistronic vector to drive the co-expression of mKate (as an expression marker) and GECIs at a near 1:1 ratio. The resting GECI brightness was indicated by the fluorescence ratio of GECI and mKate (**Fig. 1F**). Consistent with their lower Ca^{2+} affinities, the normalized brightness of NEMOc or NEMOf was only about 0.25-0.5 of GCaMP6m. This finding indicates that the lower basal fluorescence of NEMO variants might contribute to the observed large dynamic range of NEMOc or NEMOf. However, even though the dynamic ranges of NEMOm, NEMOs and NEMOb are over 5-fold higher than GCaMP6m, their basal fluorescence is either similar to or brighter than that of GCaMP6m (**Fig. 1D, 1F**). Hence, at least for these three indicators, the high dynamic range is not related to the lowering of the basal brightness. In consonance with this notion, NEMO-expressing cells with comparable basal fluorescence to those expressing GCaMP6m still exhibited larger dynamics (**Fig. 1G**). Therefore, the larger dynamic range of NEMO indicators is not a mere

reflection of lower basal fluorescence. Taken together, these results establish NEMO indicators as a class of GECIs with extraordinary large Ca^{2+}-dependent changes in fluorescence.

Using NEMOc as an example, we next set out to decipher the mechanisms underlying the superior dynamic range of NEMO sensors. In GECI proteins, such as NCaMP7(*7*) and most sensors from the GECO(*12*) and GCaMP series(*13*), the fluorophore exists in two configurations: an anionic state and a neutral state. The Ca^{2+}-induced brightening of GECI fluorescence is caused by an increase in both the proportion and molecular brightness of the anionic form(*7*) (*12*) (*13*). Similarly, the fluorophore of NEMOc exists in an anionic state, with a peak absorption at 509 nm, and a neutral state, with a maximal absorption at 403 nm (**Supplementary Fig. 2B**). The analysis of pH dependence of the absorption spectra revealed that the Ca^{2+}-induced increase in the proportion of anionic NEMOc was similar to that of NCaMP7, and smaller than that of GCaMP6m (**Supplementary Fig. 2C–E**, **Supplementary Table 4**). The Ca^{2+}-induced brightening of the anionic fluorophore of NEMOc was dramatic (292.1-fold increase), and 5–13 fold larger than that of NCaMP7 or GCaMP6m (49- and 21.3-fold increase, respectively) (**Supplementary Table 4**). However, the increase in the dynamic range was mostly associated with the considerably dimmer anionic fluorophore of NEMOc (0.22 ± 0.01 $mM^{-1}cm^{-1}$) in the absence of Ca^{2+}, which was approximately one-sixth that of NCaMP7 (1.34 ± 0.06 $mM^{-1}cm^{-1}$) and one-fifth that of GCaMP6m (1.11 ± 0.13 $mM^{-1}cm^{-1}$). The high dynamic range of NEMOc was also a result of increased brightness of Ca^{2+}-saturated anionic NEMOc (64.26 ± 2.67 $mM^{-1}cm^{-1}$), which was similar to that of NCaMP7 (65.63 ± 1.73 $mM^{-1}cm^{-1}$), and approximately three times that of GCaMP6m (23.66 ±1.22 $mM^{-1}cm^{-1}$). Overall, these findings indicate that the superior dynamic range of NEMO indicators can be explained by Ca^{2+}-induced changes in both the proportion and the absolute brightness of the anionic fluorophores of NEMO variants.

Some NEMO indicators, however, showed lower basal fluorescence (**Fig. 1F**). To examine whether it is possible to compensate weaker NEMO fluorescence with stronger illumination, we measured the photostability of NEMO sensors. mNG as the template of NEMO is more prone to photobleaching than EGFP, the FP in GCaMP6m (**Supplementary Fig. 3A**, top two panels)(*10*). However, engineered mNG-based NEMOm showed better photostability than GCaMP6m or mNG (**Supplementary Fig. 3A**). It endured nearly 40 times higher illumination than GCaMP6m, and

showed no apparent photobleaching. This property can potentially enhance the basal fluorescence of NEMO sensors by over 60-fold (**Supplementary Fig. 3A**), greatly broadening the applicability of NEMO sensors in scenarios requiring stronger light illumination. Collectively, these results established NEMO variants as highly photo-stable sensors with ultra-large dynamic ranges.

Performance of NEMO sensors in non-excitable cells

We next moved on to compare the ability of NEMO sensors to report receptor-mediated signals with frequently-used GECI sensors, including GCaMP6m, NCaMP7 and the most recently-developed jGCaMP8f (*4*). We used a submaximal dose of carbachol (CCh, 10 μM), an agonist of muscarinic acetylcholinergic receptors (mChR), to induce Ca^{2+} transients and the subsequent Ca^{2+} oscillations in HEK293 cells transfected with different GECI constructs. Peak signal-to-baseline (SBR, $\Delta F/F_0$) values of NEMOb (26.7 ± 2.2) and NEMOs (32.1 ± 2.2) were at least three times higher those of GCaMP6m (7.5 ± 0.4), jGCaMP8f (5.1 ± 0.1), and NCaMP7 (5.5 ± 0.3) (**Fig. 2A, Supplementary Fig. 3B, C**). The SBRs of NEMOm (101.9 ± 6.6), NEMOc (112.0 ± 9.8) and NEMOf (194.3 ± 7.7) were 13-25 times higher than that of GCaMP6m (**Supplementary Movie 2**). Similarly, the performance of NEMO sensors in reporting CCh-induced Ca^{2+} oscillations was also superior over jGCaMP8f and NCaMP7 (**Fig. 2A, Supplementary Fig. 3B-C**).

We further examined the performance of NEMO sensors in detecting weak Ca^{2+} signals. As a model, we used TG-induced Ca^{2+} release and the SOCE response. In this scenario, the peak SBR value of NEMO sensors was found to be at least 5 times higher than that of NCaMP7 (**Fig. 2B, Supplementary Fig. 3D**). We also tested their capability to monitor Ca^{2+} transients generated via activation of the *Bombyx mori* gustatory receptor (BmGr-9), which is known to be much smaller than SOCE in terms of the Ca^{2+} signal amplitude(*14*). Similarly, the NEMO response was much stronger than that of GCaMP6s (**Fig. 2C**). Taken together, intensiometric changes of NEMO sensors in response to the investigated Ca^{2+} signals in non-excitable cells are remarkably larger than those of other GECI sensors tested in our side-by-side comparison.

One major drawback of intensiometric Ca^{2+} sensors is that they could not be employed to directly report Ca^{2+} concentration. We thus asked whether NEMO sensors bear some photochemical

features to allow the measurements of absolute Ca^{2+} concentrations. To this end, we first explored the use of NEMO as ratiometric sensors. The apoNEMO variant has a small but appreciable excitation peak at 403 nm (**Supplementary Fig. 2A**). Furthermore, the fluorescence of apoNEMOs excited by 405 nm light (F_{405}) was brighter than its Ca^{2+}-bound form. *In vitro* Ca^{2+} titration revealed that the F_{405} response of NEMOs decreased as a function of increasing Ca^{2+} concentration with an apparent K_d of 234 ± 15 nM, as opposed to the Ca^{2+}-induced enhancement of NEMOs fluorescence excited by 490 nm light (F_{490}) (**Supplementary Fig. 4A**). Consequently, the dynamic range indicated by the F_{490}/F_{405} ratio was 3.4-fold higher than that obtained with F_{490} only (**Supplementary Fig. 4B**). A similar trend was also visualized in HEK293 cells expressing NEMOs, with the ratiometric dynamic range significantly larger than intensiometric ones (**Fig. 2D, Supplementary Fig. 4C-D**).

While performing ratiometric recordings, we noticed that UV illumination approximately doubled the fluorescence intensities of NEMO sensors under low Ca^{2+} conditions, indicating the existence of a photochromic effect (*15*) (**Supplementary Fig. 4E**). We thus asked whether NEMO indicators could also report Ca^{2+} concentration with a newly-developed intermittent photochromism-enabled absolute quantification (iPEAQ) method (*15*), which allows measurements of Ca^{2+} levels independent on GECI concentration and the intensity of excitation light. Indeed, we found that NEMOf exhibited photochromic characteristics. Exposure of NEMOf to UV light could increase its fluorescence in an inversely Ca^{2+} dependent manner, with approximately 50-fold increase under Ca^{2+}-free condition (**Supplementary Fig. 4F-G**). We then quantified Ca^{2+} release induced by submaximal stimulation of mChR with the iPEAQ approach, and found that the resulting Ca^{2+} transients could reach up to 4.4 μM (**Fig. 2E**). Collectively, NEMO sensors can also be used as ratiometric or photochromic indicators(*15*), not only reporting Ca^{2+} signals with an improved resolution of amplitude, but also directly indicating basal Ca^{2+} levels.

Performance of NEMO sensors in neurons *ex vivo*

We next examined the responses of NEMO sensors in cultured neurons dissociated from fetal rat hippocampus. We excited neurons that expressed different GECI constructs using electrical field

stimulation, and measured the corresponding changes in fluorescence signals of the sensors (**Fig. 3**). We observed that all NEMO sensors were sensitive enough to detect Ca^{2+} signals elicited by even a single action potential (AP) (**Fig. 3A**), with peak SBR approximately twice higher than GCaMP6s (0.12 ± 0.01) or GCaMP6f (0.11 ± 0.03). Consistent with the *in vitro* analysis demonstrating that the K_{off} of NEMOf was higher than that of GCaMP6f (**Supplementary Table 3**), NEMOf was fast enough to distinguish neuron responses induced by electrical field stimulation with a frequency up to 5 Hz (**Fig. 3B**). These observations indicate that NEMO sensors perform similarly or better than existing state-of-the-art EGFP-based sensors in terms of single-AP detection sensitivity and response time.

Similar to what we observed in non-excitable cells, the ultra-high dynamic range of NEMO sensors enabled high-resolution detection of Ca^{2+} signals of various amplitudes. In response to a 5 Hz field stimulation, the peak amplitude of NEMOf response (2.9 ± 0.5 $\Delta F/F_0$) was approximately three times that of GCaMP6f, placing NEMOf among the most sensitive and fast GECIs that include XCaMP(*16*), jGCaMP7(*9*), or jGCaMP8 series(*4*). As the stimulus frequency increased, the difference between peak NEMOf signal and GCaMP6f became more pronounced. For example, NEMOf response induced by 10 Hz simulation was approximately 5 times that of GCaMP6f (**Fig. 3C**), while the peak NEMOf signal in response to 180 Hz stimulation was 22.7 times that of GCaMP6f (**Fig. 3D**). Over the entire range of stimulus intensities tested, the responses of all NEMO sensors were significantly stronger than those of GCaMP6s, GCaMP6f, and jGCaMP8f (**Fig. 3D**). The NEMO sensors also reported the frequency of the stimulus in a fairly linear manner, with no apparent saturation even up to 180 Hz (**Fig. 3E**), indicating that NEMO sensors are suitable for resolving neuronal Ca^{2+} dynamics in response to the full spectrum of activities under physiological conditions.

We further tested NEMO sensors in cortical neurons in acutely-prepared mouse brain slices using two-photon imaging with whole-cell patch clamp electrophysiological recording. We transfected layer 2/3 neurons in the primary visual cortex (V1) with adeno-associated virus (AAV) in which GECI expression was driven by the human synapsin I promoter, a neuron-specific promoter (AAV-hsyn1-GECI constructs), through a stereotaxic injection. Three weeks later, cytoplasmic fluorescence was detectable in the majority of layer 2/3 neurons. AP was elicited by intracellular

injection of current pulse train via the recording micropipette, and the corresponding signals of GECI sensors were recorded and compared (**Supplementary Fig. 5A**, left panel). Under a whole-cell patch clamp condition, the intracellular environment could be perturbed and the GECI signal was diluted (*16*). Despite of this caveat, the response of all NEMO sensors induced by AP occurring at 50 Hz or higher was significantly higher than that of GCaMP6s or GCaMP6f (**Supplementary Fig. 5A**, middle panel). Consistent with data obtained using dissociated neurons, the response of NEMO sensors was significantly more pronounced under most tested conditions, with NEMOf exhibiting the fastest kinetics (**Supplementary Fig. 5A**, middle and right panel).

Of note, most fast GECI sensors developed to date (e.g., RCaMP2(*17*), jRGECO1a(*18*), XCaMP-Gf(*16*), and jGCaMP8f(*4*)) display rather limited dynamic ranges. By contrast, NEMOf expressed in both non-excitable and excitable cells shows fast and ultra-high dynamic range, making it an ideal tool to decode fast and highly dynamic Ca^{2+} signals in living cells and tissues.

In vivo performance of NEMO sensors in mice

We next tested the performance of NEMO sensors in the V1 neurons *in vivo* using two-photon microscopy (**Fig. 4A**). Three weeks after transfection with AAV-hsyn1-GECI constructs, we presented drifting grating stimulus to one eye of anesthetized mice to evoke spiking activity of layer 2/3 neurons in the contralateral V1(*19*), and then monitored the corresponding fluorescence transients of GECI sensors in these neurons evoked by the visual stimulus. To ensure direct comparison with GCaMP6 sensors, we used 920 nm light, an excitation wavelength optimized for GCaMP but less ideal for NEMO (980 nm) to excite the GECIs.

All the tested indicators accurately reported differential changes in response to different orientations or direction of visual stimuli (**Fig. 4B, Supplementary Fig. 5B-C**). Consistent with *in vitro* characterization, NEMOs was relatively slow, with half decay time similar to that of GCaMP6s (1.36 ± 0.08 s). The half decay time of NEMOs was 1.17 ± 0.03 s, slightly shorter than that of GCaMP6s ($p < 0.02$, *t*-test). NEMOf was the fastest among all NEMO variants, with the half decay time (409 ± 54 ms) similar to that of GCaMP6f (482 ± 48 ms) (**Supplementary Fig. 5D**).

We then moved on to compare the sensitivity of GECIs. When examined by the fraction of

responsive cells (**Supplementary Fig. 5E**), no significant difference between NEMO variants and corresponding GCaMP6 indicators was detected. However, considering the peak fluorescence response, the cumulative distribution of peak $\Delta F/F_0$ of NEMOm and NEMOs was substantially right-shifted relative to the GCaMP6 signal (**Fig. 4C**), indicating that NEMOm and NEMOs are more responsive. The median response of NEMOs ($\Delta F/F_0$ =3) was over 4 and 7 times stronger than that of GCaMP6s ($\Delta F/F_0$ = 0.73) and GCaMP6f ($\Delta F/F_0$ = 0.44), respectively. The visual-stimuli-induced response reported by NEMOs was much larger than existing values reported by sensitive GECIs such as jRGECO1a(*18*), jYCaMP1s(*20*), jGCaMP7s(*9*) and jGCaMP8s(*4*). In parallel, the median response of NEMOf ($\Delta F/F_0$ = 0.80) was significantly larger than that of GCaMP6f ($\Delta F/F_0$ = 0.44) (right panel in **Fig. 4B** vs **Supplementary Fig. 5B**, left panel), as well as those reported by the known fastest GECIs such as R-CaMP2(*17*), jRGECO1a(*18*), jGCaMP7f(*9*) and jGCaMP8f (*4*).

In addition, NEMOs showed good basal fluorescence in the mouse V1 that was comparable to that of GCaMP6s even under excitation conditions optimized for GCaMP (**Supplementary Fig. 6A-B**). When illuminated using light of longer wavelength at 980 nm, the basal fluorescence of the NEMOf sensor increased without compromising its performance (**Supplementary Fig. 6C, D**). Thus, for NEMOf and NEMOc that exhibit weaker basal fluorescence, their excitation by light with optimized wavelength and intensity (**Supplementary Fig. 3A**) might further improve the signal to noise ratio.

Lastly, we recorded the fluorescence response of NEMOs in neurons deeply buried in the mouse brain using fiber photometry and settings optimized for GCaMP recordings (*21*). For the experiment, neurons within the corpus striatum were infected with AAV-hsyn1-NEMOs or AAV-hsyn1-GCaMP6f. Two weeks later, the GECI fluorescence signal excited by 410 nm (F_{410}) or 470 nm light (F_{470}) was collected, and Ca^{2+} responses within the neurons elicited by tail-pinching stimulus were evaluated using the F_{470}/F_{410} ratio (R) (**Fig. 4D**). Even though the near-UV light (410 nm) excitation reduced the dynamics of NEMO and the 470 nm light was not optimal for NEMOs excitation (**Supplementary Fig. 2A** and **Supplementary Fig. 4D**), the NEMOs-reported Ca^{2+} transients evoked by the sensory stimulus were significantly larger than those of GCaMP6f (**Fig. 4E**), with the median peak response of NEMOs approximately 3 times that of GCaMP6f ($\Delta R/R_0$: 20.2 vs 6.5). Collectively, NEMOs and NEMOf are among the most sensitive GECI tools for *in vivo*

monitoring of both slow and fast neural activities.

Conclusions

In the current study, we have reported a series of GECIs with greatly improved photochemical properties. Unlike current state-of-the-art indicators that partially sacrifice the dynamic range for improved sensitivity and/or faster kinetics, NEMO variants are fast acting while still retaining ultra-high dynamic ranges to report Ca^{2+} signaling both *ex vivo* and *in vivo*. They are more versatile than the most popular GCaMP series, allowing simultaneous imaging with cyan fluorescence and exhibiting higher photostability that can endure substantially stronger illumination, thereby meeting the demand for varying basal fluorescence under different circumstances. Overall, the ultra-sensitive NEMO variants may serve as the tool-of-choice for monitoring Ca^{2+} dynamics in mammalian cells or neural activities *in vivo*.

ACKNOWLEDGMENTS

This work was supported by the National Natural Science foundation of China (91954205 to Y.W.; 32130043 and 32071025 to X.Z.; 31872759 to A.-H. T.; 31971095 to L.H.; 32171033 to D. X.; and 91854209 to S.W.), the National Key Research and Development Program of China (2020YFA0112200to A.-H. T.), and the Ministry of Science and Technology of China (grant 2019YFA0802104 to Y.W.), and China postdoctoral Science Foundation (grant 2021M703089 to JC).

Author contributions

YW, XZ, AT, LH and DX supervised and coordinated the study. JL designed and generated all the plasmid constructs. JL and WG performed the *in vitro* assays. JL performed all fluorescence imaging in HEK cells, with help from WG and LW. JC performed confocal imaging of dissociated neurons. TH performed confocal imaging on isolated cardiac cells. LY performed two-photon imaging of whole-cell patched neurons in mouse brain slices. ZS performed *in vivo* two-photon imaging of visual cortical neurons in mice. XS monitored basal fluorescence of indicators in mice visual cortex. XY performed fiber photometry *in vivo*. JL, ZS, JC, WG, LW, LY, ZS, XY and XS analyzed data, with input from the other authors. DLG and SW provided intellectual input to the manuscript. YZ and YW wrote the manuscript with inputs from all the other authors.

References

1. M. J. Berridge, P. Lipp, M. D. Bootman, The versatility and universality of calcium signalling. *Nat Rev Mol Cell Biol* **1**, 11 (Oct, 2000).
2. M. Z. Lin, M. J. Schnitzer, Genetically encoded indicators of neuronal activity. *Nature neuroscience* **19**, 1142 (Aug 26, 2016).
3. V. Perez Koldenkova, T. Nagai, Genetically encoded Ca^{2+} indicators: properties and evaluation. *Biochimica et biophysica acta* **1833**, 1787 (Jul, 2013).
4. M. R. Y. Zhang, D. Bushey, J. Zheng, D. Reep, G. J. Broussard, A. Tsang, G. Tsegaye, , S. N. R. Patel, J. X. Lim, R. Zhang, M. B. Ahrens, G. C. Turner, S. S.-H. Wang, K. , W. K. Svoboda, E. R. Schreiter, J. P. Hasseman, I. Kolb, L. L. Looger, jGCaMP8 fast genetically encoded calcium indicators. (2020).
5. Y. Zhao *et al.*, An expanded palette of genetically encoded Ca^{2+} indicators. *Science* **333**,

1888 (Sep 30, 2011).
6. T. W. Chen *et al.*, Ultrasensitive fluorescent proteins for imaging neuronal activity. *Nature* **499**, 295 (Jul 18, 2013).
7. O. M. Subach *et al.*, Novel Genetically Encoded Bright Positive Calcium Indicator NCaMP7 Based on the mNeonGreen Fluorescent Protein. *International journal of molecular sciences* **21**, (Feb 28, 2020).
8. Y. Nasu, Y. Shen, L. Kramer, R. E. Campbell, Structure- and mechanism-guided design of single fluorescent protein-based biosensors. *Nature chemical biology* **17**, 509 (May, 2021).
9. H. Dana *et al.*, High-performance calcium sensors for imaging activity in neuronal populations and microcompartments. *Nat Methods* **16**, 649 (Jul, 2019).
10. N. C. Shaner *et al.*, A bright monomeric green fluorescent protein derived from Branchiostoma lanceolatum. *Nat Methods* **10**, 407 (May, 2013).
11. K. Horikawa, Recent progress in the development of genetically encoded Ca^{2+} indicators. *J Med Invest* **62**, 24 (2015).
12. R. S. Molina *et al.*, Understanding the Fluorescence Change in Red Genetically Encoded Calcium Ion Indicators. *Biophysical journal* **116**, 1873 (May 21, 2019).
13. L. M. Barnett, T. E. Hughes, M. Drobizhev, Deciphering the molecular mechanism responsible for GCaMP6m's Ca^{2+}-dependent change in fluorescence. *PLoS One* **12**, e0170934 (2017).
14. K. Sato, K. Tanaka, K. Touhara, Sugar-regulated cation channel formed by an insect gustatory receptor. *Proceedings of the National Academy of Sciences of the United States of America* **108**, 11680 (Jul 12, 2011).
15. F. Bierbuesse *et al.*, Absolute measurement of cellular activities using photochromic single-fluorophore biosensors and intermittent quantification. *Nature communications* **13**, 1850 (Apr 6, 2022).
16. M. Inoue *et al.*, Rational Engineering of XCaMPs, a Multicolor GECI Suite for In Vivo Imaging of Complex Brain Circuit Dynamics. *Cell* **177**, 1346 (May 16, 2019).
17. M. Inoue *et al.*, Rational design of a high-affinity, fast, red calcium indicator R-CaMP2. *Nature methods* **12**, 64 (Jan, 2015).
18. H. Dana *et al.*, Sensitive red protein calcium indicators for imaging neural activity. **5**, (Mar 24, 2016).
19. C. M. Niell, M. P. Stryker, Highly selective receptive fields in mouse visual cortex. *The Journal of neuroscience : the official journal of the Society for Neuroscience* **28**, 7520 (Jul 23, 2008).
20. M. A. Mohr *et al.*, jYCaMP: an optimized calcium indicator for two-photon imaging at fiber laser wavelengths. *Nature methods* **17**, 694 (Jul, 2020).
21. G. Cui *et al.*, Deep brain optical measurements of cell type-specific neural activity in behaving mice. *Nature protocols* **9**, 1213 (2014).

Figures Legends

Figure 1. *In cellulo* screening of optimized NEMO indicators and their *in vitro* characterization. A) NEMO sensors are generated by introducing amino acid substitutions in NCaMP7. Top panel, a diagram showing the design of NEMO variants; a table (middle panel) or NCaMP7 structure (*7*) (bottom panel) showing key amino acids substitutions introduced into NCaMP7 to generate NEMO variants. B–E) Screening of GCaMP and NCaMP7 variants in HEK-293 cells. B) Ca^{2+} imaging-based screening. A typical trace from NCaMP7-expressing cells is shown. To avoid saturation of the camera, after recording the rest fluorescence (F_0) with regular exposure time (approximately 500 ms), time-series for variants with high dynamic range were recorded using one-tenth to one-fifth the exposure time. Afterwards, the fluorescence response curves of each cell were scaled up according to the corresponding F_0. After recording F_0, endoplasmic reticulum Ca^{2+} store was depleted using 2.5 μM ionomycin and 1 μM thapsigargin. Then, the cells were incubated in an imaging solution containing 300 μM EGTA, to read minimal GECI fluorescence (F_{min}). Finally, the cells were exposed to imaging solution containing 100 mM Ca^{2+} to obtain the maximal response (F_{max}) via store-operated Ca^{2+} entry. C) Representative traces of GCaMP6m and NCaMP7 (left), or selected NEMO sensors (right). D) Scatter diagram of F_0–mean dynamic range (F_{max}/F_{min}) of the screened constructs. E) *In vitro* dose–response curves of NEMO sensors. Top, typical traces; Bottom, statistics (see Supplemental Table 3 for details) (n=3, at least 4 parallel samples per repeat). F) Basal fluorescence of NEMO or NCaMP7 sensors relative to that of GCaMP6m. G) F_0–dynamic range of individual cells expressing NEMO variants or GCaMP6m.

Figure 2. Performance of transiently expressed NEMO sensors in non-excitable HEK-293 cells. A) Typical Ca^{2+} oscillations induced by carbachol (CCh, 10 μM), as indicated by GCaMP6m, NCaMP7, and NEMO sensors. n = 3, with at least 15 cells per repeat. B) Ca^{2+} release and store-operated Ca^{2+} entry (SOCE) responses induced by thapsigargin (TG). n = 3, with at least 20 cells per repeat. C) Fructose-elicited response in cells co-expressing BmGr-9, an insect fructose receptor. Left, typical traces; right, statistics ($p < 0.0001$, Student's *t*-test). n = 3, with at least 9 cells per repeat. D-E) Measurements of Ca^{2+} concentration with NEMO sensors. D) Ratiometric measurements with NEMOs. NEMOs transients in cells upon excitation by 488 nm or 405 nm light,

induced by 100 μM CCh. Left, typical NEMOs fluorescence response excited by 488 nm light or 405 nm light. Right, representative intensiometric (black) or ratiometric (red, F_{488ex}/F_{405ex}) responses of the same set of cells as those shown on the left. n = 3, with at least 16 cells per repeat. E) Intermittent photochromism-enabled absolute quantification (iPEAQ) of Ca^{2+} levels. Shown are fluorescence intensity (purple) and [Ca^{2+}] traces (green) of NEMOf-expressing cells in response to 10 μM CCh. *In vitro* calibration to determine the absolute Ca^{2+} concentration, or [Ca^{2+}], was shown in Supplementary Fig. 4G. n = 3, with at least 9 cells per repeat.

Figure 3. Responses of NEMO variants in dissociated rat hippocampus neurons excited by electric field stimulation. A) Average responses elicited by 1 Hz stimulation. B, C) Mean NEMOf and GCaMP6f transients induced by 5 Hz (B) or 10 Hz (C) stimulation. D) Mean GECI responses elicited by stimulation at different frequency. Inset, enlarged view of responses of reference GECI sensors (SBR magnified 9 times). E) Statistics for data shown in panels A and D. Each GECI measurement set was analyzed from multiple dendrites of at least 10 neurons in three different primary hippocampal neuron cultures.

Figure 4. *In vivo* performance of NEMO sensors in mouse neurons infected with GECI-encoding adeno-associated virus (AAV). A–C) Responses of neurons in the visual cortex in mouse induced by a visual stimulus. A) Diagram showing the experimental setups for two-photon imaging of neurons in response to drift gratings. B) Typical responses. C) Cumulative distribution of peak signal-to-baseline-ratio (SBR) transients of GECI sensors. D–F) Ratiometric response of GCaMP6f and NEMOs in neurons in the corpus striatum in mouse recorded using fiber photometry. D) Diagram of the experimental setup for fiber photometry recordings. E) Mean ratiometric response elicited by pinch stimulation at mouse tail tip. Left, mean traces; right, statistics ($p < 0.0001$, *t*-test). NEMOs, data for 101 cells from 6 mice; GCaMP6f, data for 97 cells from 6 mice. F) Cumulative distribution of peak responses shown in E (p = 1.6E-21, Kolmogorov–Smirnov test).

Figure 1

A

	L1	CaM	L3	L4
NCaMP7	N/A	Q3-A15-M36	GGSGGGSSS	MYF
NEMOs	GITLGMDELYK	Q3-A15-M36	GGSGGGSSS	IYF
NEMOb	GGS	Q3-A15-M36	GGSGGGSSS	IYF
NEMOf	GGS	D3-E15-F36	GGGGS	IYF
NEMOc	N/A	Q3-A15-M36	GGGGS	IYF
NEMOm	GGS	Q3-A15-M36	GGSGGS	IYF

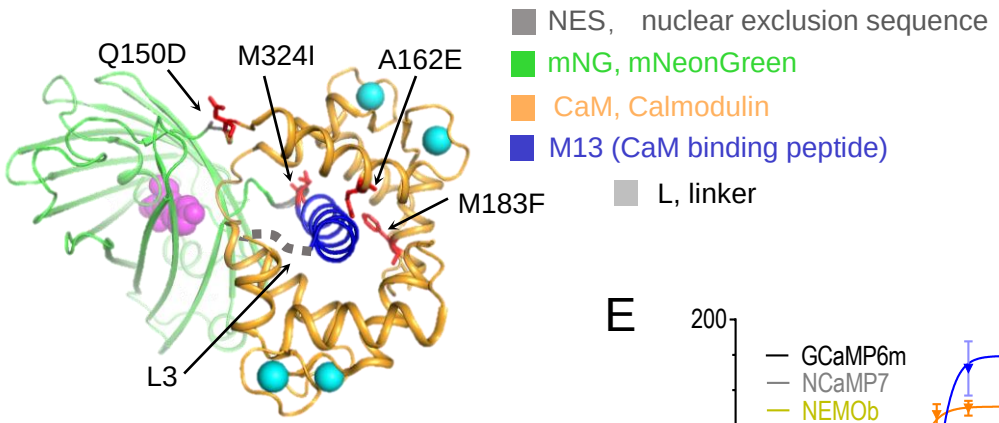

B

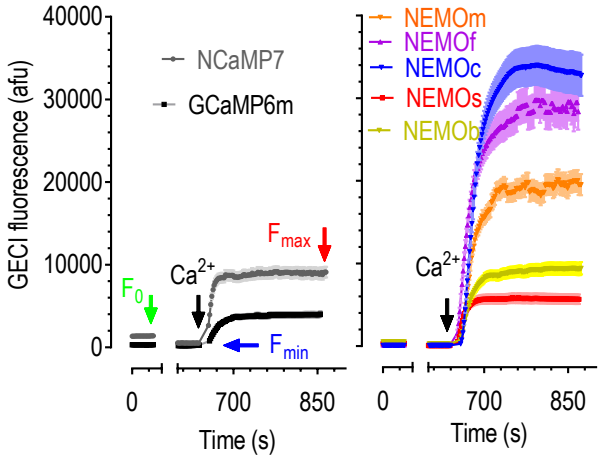

C

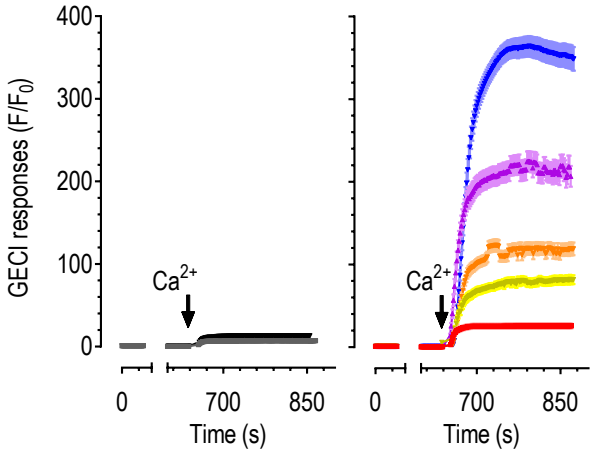

D

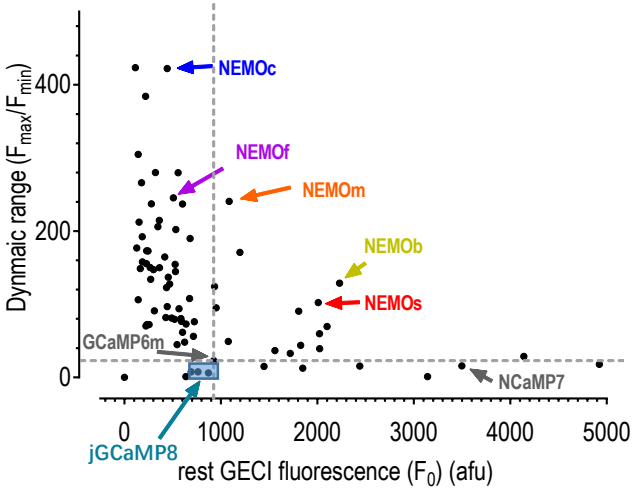

E

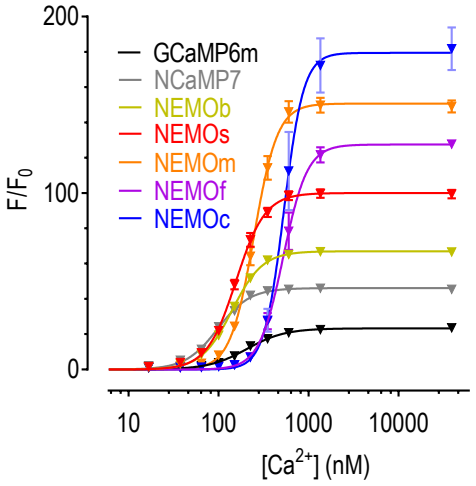

	K_d (nM)	$Hill_n$
NEMOs	156±4	2.7±0.2
NEMOb	141±1	2.6±0.1
NEMOf	528±17	3.2±0.3
NEMOc	557±16	3.8±0.4
NEMOm	248±4	3.3±0.1

F

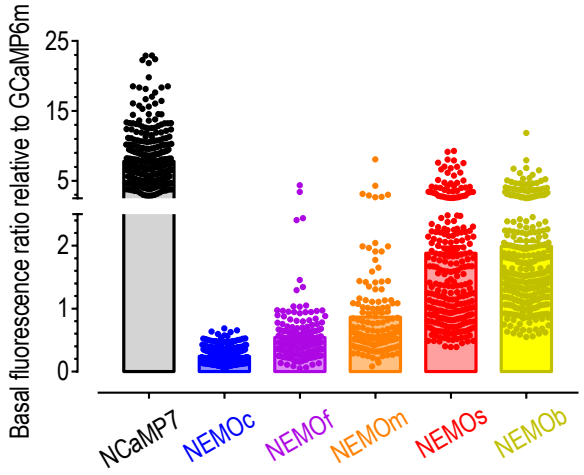

G

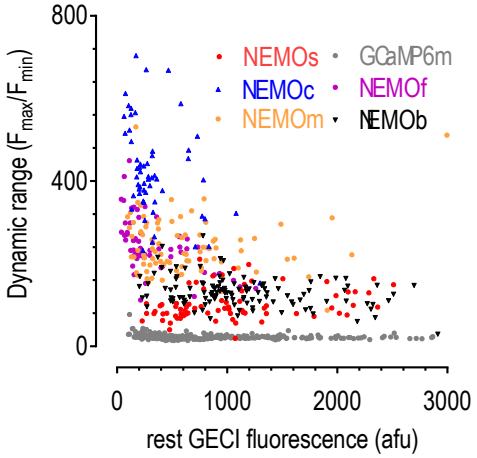

Figure 2

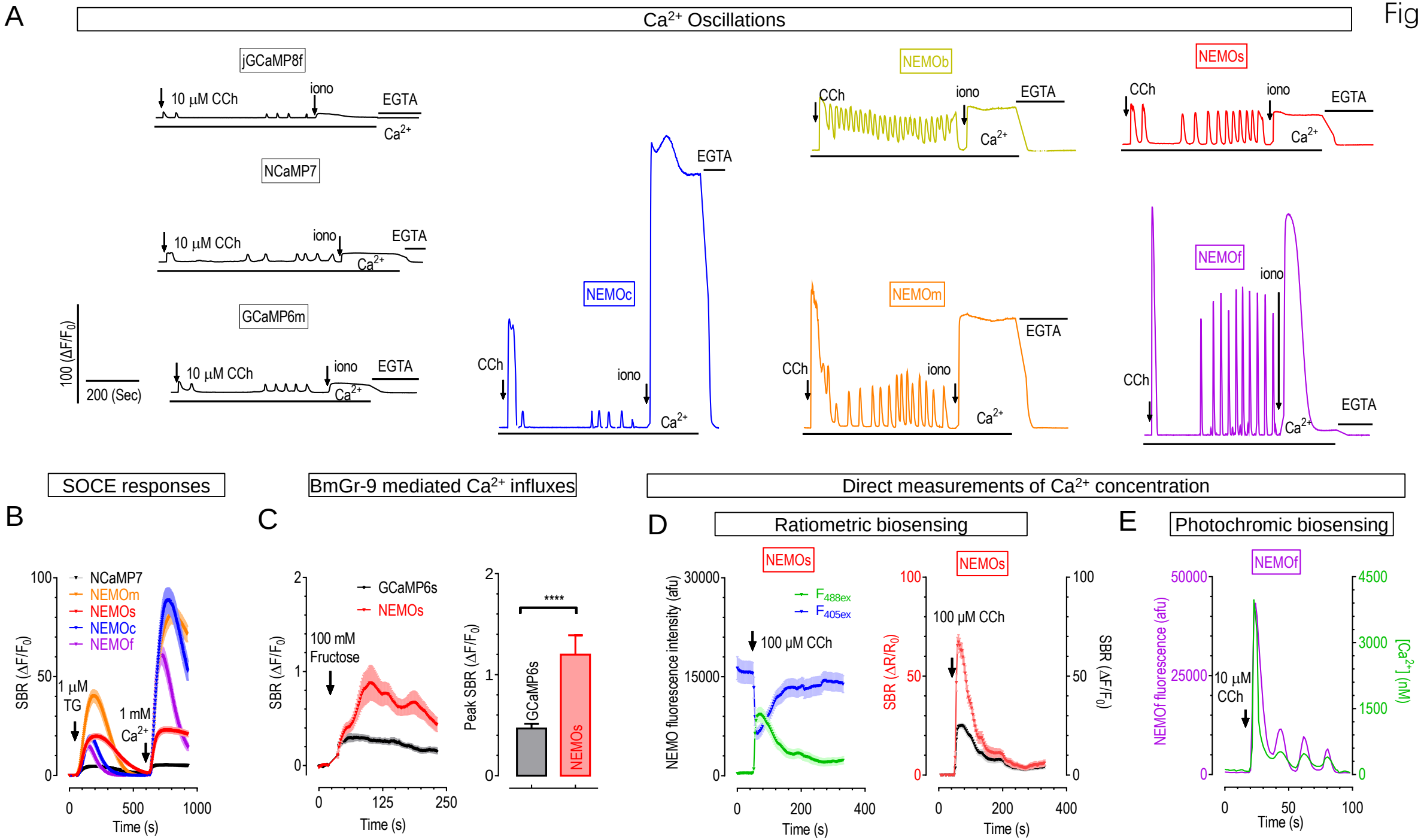
A
Ca2+ Oscillations
jGCaMP8f
10 μM CCh
iono
EGTA
Ca2+
NCaMP7
GCaMP6m
100 (ΔF/F0)
200 (Sec)
NEMOc
NEMOb
NEMOs
NEMOm
NEMOf
CCh
SOCE responses
B
NCaMP7
NEMOm
NEMOs
NEMOc
NEMOf
SBR (ΔF/F0)
1 μM TG
1 mM Ca2+
Time (s)
BmGr-9 mediated Ca2+ influxes
C
GCaMP6s
NEMOs
100 mM Fructose
Peak SBR (ΔF/F0)
****
Direct measurements of Ca2+ concentration
D
Ratiometric biosensing
NEMO fluorescence intensity (afu)
F488ex
F405ex
100 μM CCh
SBR (ΔR/R0)
SBR (ΔF/F0)
E
Photochromic biosensing
NEMOf fluorescence (afu)
10 μM CCh
[Ca2+] (nM)

Figure 3

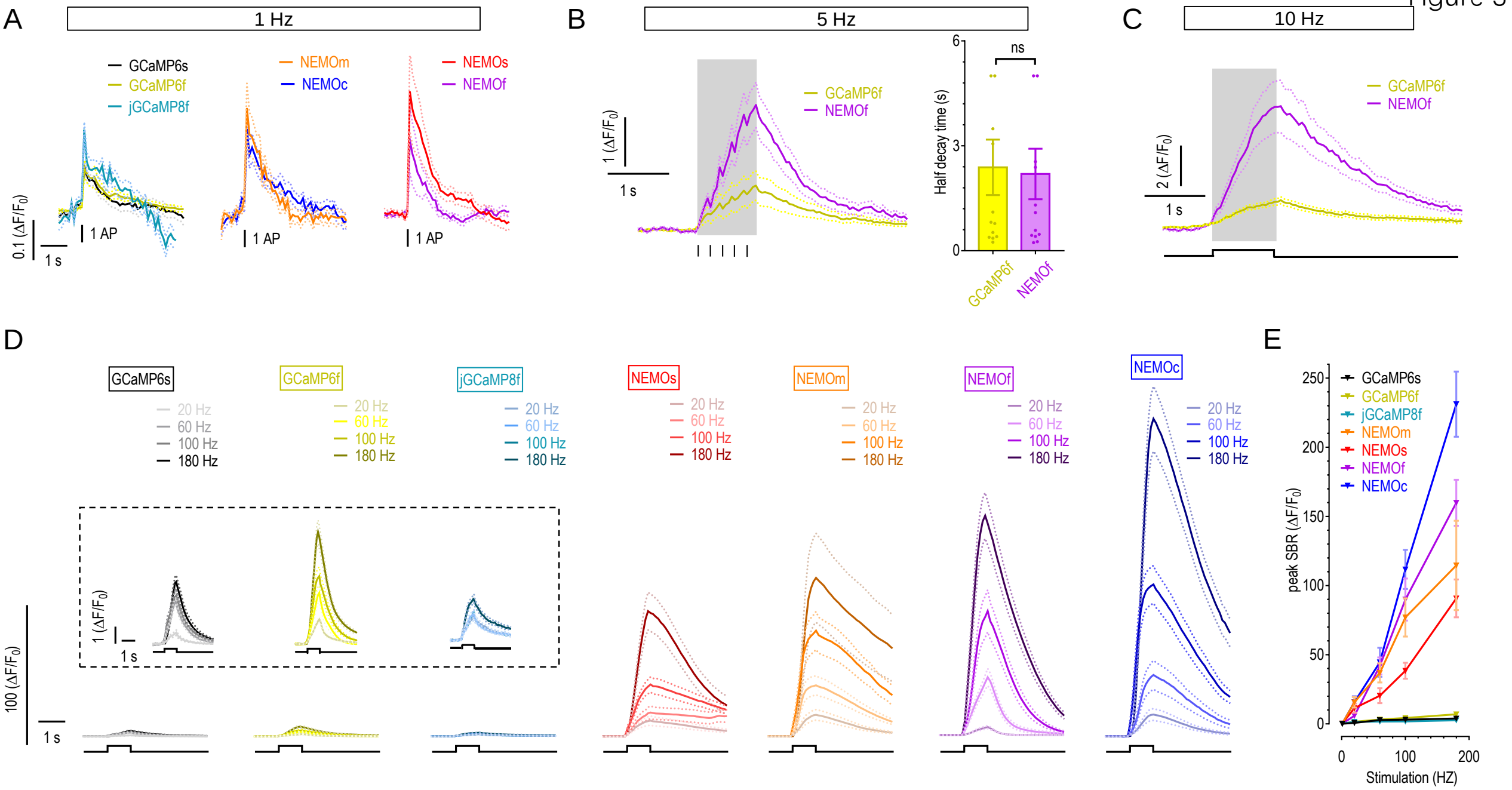
A
1 Hz
GCaMP6s
GCaMP6f
jGCaMP8f
NEMOm
NEMOc
NEMOs
NEMOf
0.1 (ΔF/F0)
1 AP
1 s
B
5 Hz
1 (ΔF/F0)
1 s
Half decay time (s)
ns
C
10 Hz
2 (ΔF/F0)
D
20 Hz
60 Hz
100 Hz
180 Hz
100 (ΔF/F0)
E
peak SBR (ΔF/F0)
Stimulation (HZ)

Figure 4

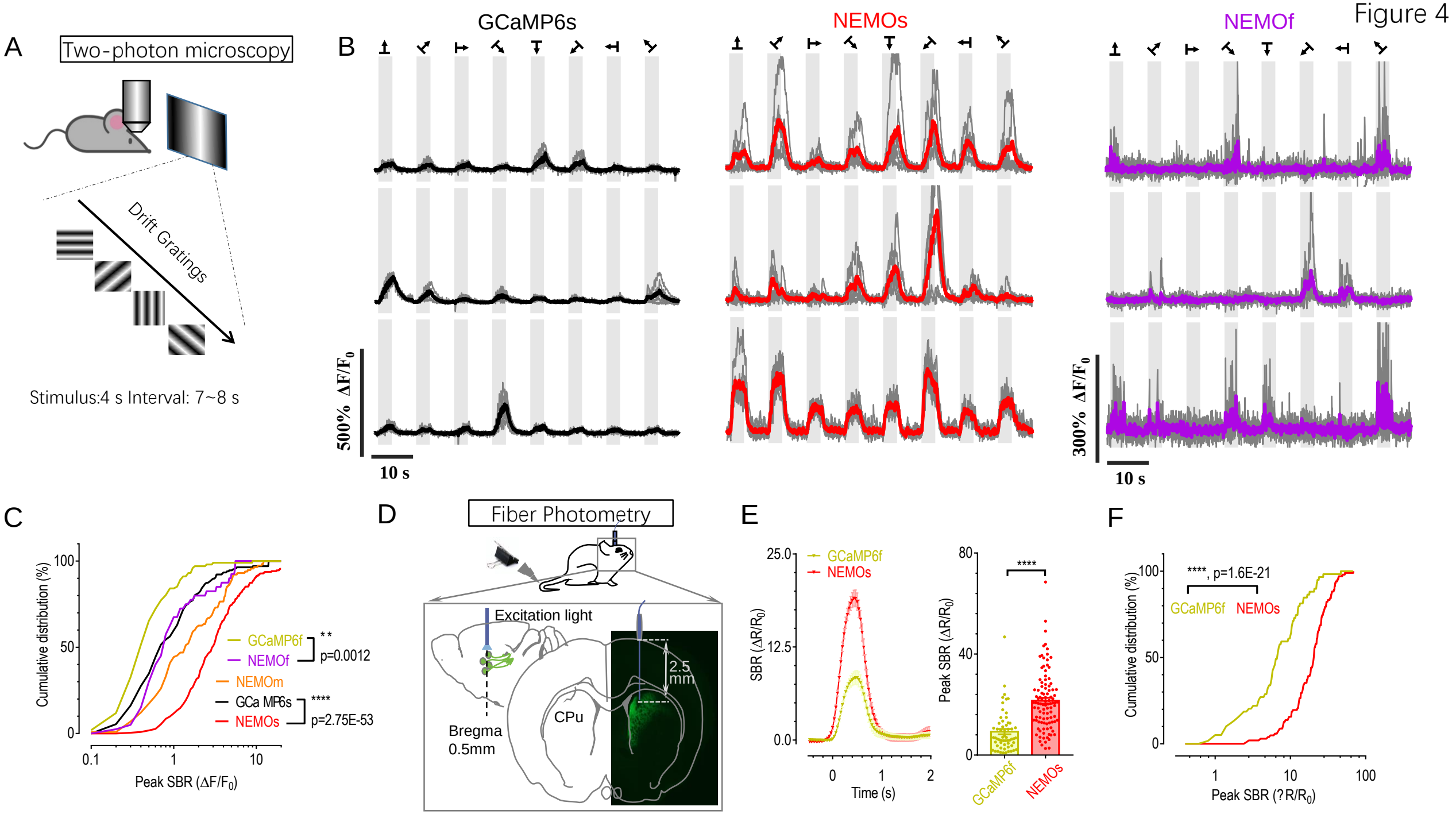
A
Two-photon microscopy
Drift Gratings
Stimulus:4 s Interval: 7~8 s
B
GCaMP6s
NEMOs
NEMOf
500% ΔF/F0
10 s
300% ΔF/F0
10 s
C
Cumulative distribution (%)
Peak SBR (ΔF/F0)
GCaMP6f
NEMOf
NEMOm
GCa MP6s
NEMOs
**
p=0.0012
****
p=2.75E-53
D
Fiber Photometry
Excitation light
Bregma
0.5mm
CPu
2.5
mm
E
GCaMP6f
NEMOs
SBR (ΔR/R0)
Time (s)
Peak SBR (ΔR/R0)
****
GCaMP6f
NEMOs
F
****, p=1.6E-21
GCaMP6f
NEMOs
Cumulative distribution (%)
Peak SBR (?R/R0)